



CT&F - Ciencia, Tecnología y Futuro

ISSN: 0122-5383

Instituto Colombiano del Petróleo (ICP) - ECOPETROL S.A.

Riaño Z, J. Sebastian; Guevara L, Marco A; Belalcazar C, Luis C
CFD modeling and evaluation of a bi-stable micro-diverter valve
CT&F - Ciencia, Tecnología y Futuro, vol. 8, no. 1, 2018, pp. 77-84
Instituto Colombiano del Petróleo (ICP) - ECOPETROL S.A.

DOI: <https://doi.org/10.29047/01225383.94>

Available in: <https://www.redalyc.org/articulo.oa?id=46558133007>

- How to cite
- Complete issue
- More information about this article
- Journal's webpage in [redalyc.org](https://www.redalyc.org)

UAEH [redalyc.org](https://www.redalyc.org)

Scientific Information System Redalyc
Network of Scientific Journals from Latin America and the Caribbean, Spain and Portugal

Project academic non-profit, developed under the open access initiative

ARTICLE INFO:

Received : June 12, 2016

Revised : September 04, 2017

Accepted : October 26, 2017

CT&F - Ciencia, Tecnología y Futuro Vol 8, Num 1 June 2018. pages 77 - 84

DOI : <https://doi.org/10.29047/01225383.94>

CFD MODELING AND EVALUATION OF A BI-STABLE MICRO-DIVERTER VALVE

■ EVALUACIÓN Y MODELAMIENTO EN CFD DE UNA MICRO VÁLVULA DE DESVÍO BI-ESTABLE

Riaño Z., J. Sebastian^a; Guevara L., Marco A^{a,b*}; Belalcazar C., Luis C.^a

ABSTRACT

Micro-diverter valves are innovative and efficient devices used to generate microbubbles that can significantly enhance process efficiency in industry. Micro-diverter valves have been experimentally tested and modeled using CFD in previous works. However, a detailed CFD modeling evaluation of these valves has not been performed employing detailed turbulence modeling at transient and steady state. This article presents a three-dimensional CFD simulation and performance evaluation of a bi-stable diverted valve for microbubble generation. In the model, transient and steady state approaches were used to quantify the behavior in the valve. The $\kappa - \epsilon$ standard and $\kappa - \epsilon$ RNG turbulence models were used and compared. Different mesh configurations, mesh generation methods, and both turbulence models were evaluated to find the best set-up to simulate this valve. A brief analysis of the time-step size using the Courant number approach was also performed. Operation conditions at low Reynolds (3800) and high frequency (200 Hz) were used to assess possible industrial applications, thus setting the base for further studies. The results of this work show that at low Reynolds numbers and high frequencies, the valve is able to divert the fluid and thus it may have wider industrial applications.

RESUMEN

Las válvulas de micro-desviación son dispositivos innovadores y eficientes que se utilizan para generar microburbujas que pueden mejorar significativamente la eficiencia de un proceso en la industria. Las válvulas de microdesviación han sido probadas experimentalmente y modeladas usando CFD en trabajos previos. Sin embargo, hasta el momento no se había llevado a cabo una evaluación del modelado en CFD de estas válvulas utilizando un modelo detallado de turbulencia en estado transitorio y estable. Este artículo presenta una simulación tridimensional de CFD y la evaluación del rendimiento de una válvula desviada biestable para la generación de microburbujas. En el modelo, fueron utilizados aproximaciones en estado estable y transitorio para cuantificar el desempeño de la válvula. Los modelos $\kappa - \epsilon$ estándar y de

turbulencia $\kappa - \epsilon$ RNG fueron utilizados y comparados. Fueron evaluados diferentes métodos de generación y configuraciones de malla y ambos modelos de turbulencia para encontrar la mejor configuración para simular esta válvula. Además se realizó un breve análisis del tamaño del paso de tiempo utilizando el enfoque del número Courant. Fueron evaluadas las condiciones de operación a bajo Reynolds (3800) y alta frecuencia (200 Hz) para posibles aplicaciones industriales, sentando así la base para estudios posteriores. Los resultados de este trabajo muestran que a bajos números de Reynolds y altas frecuencias, la válvula puede desviar el fluido y, por lo consiguiente puede servir en una amplia cantidad de aplicaciones industriales.

KEYWORDS / PALABRAS CLAVE

Microfluidics | Turbulence | Diverter valve |
Microbubbles | CFD | Process Engineering.
Micro fluidos | Turbulencia | Válvula de desvío |
Microburbujas CFD | Ingeniería de Procesos.

AFFILIATION

^a Universidad Nacional de Colombia – Sede Bogotá,
Departamento de Ingeniería Química y Ambiental, C.P 111321, Bogotá, Colombia.
^b Process Engineering Department, Smart and Simple Engineering – S&S S.A.S.,
C.P 111321, Bogotá, Colombia.
*email: maguevaral@unal.edu.co

1. INTRODUCTION

Bubble bed bioreactors are important for the food industry, bioprocesses, pharmaceuticals, oil chemistry, bio fuels purification, wastewater and effluents treatment [1]–[3]. Recently, these devices have gained great interest due to their versatility and application potential. In a bioreactor, a gas phase is bubbled through a liquid bed to induce mass transfer. A bioreactor efficiency depends on the available surface area [4], [5]. Therefore, to enhance mass transfer it is necessary to reduce bubble diameter in an efficient manner [6]–[8]. One possible method to reduce bubble size is to use micro diverter valves to feed the gas to the system [1]. Micro-diverter valves limit bubble growth using an oscillatory gas flow supply [9].

Micro-diverter valves have been tested at Reynolds numbers between 800 to 15000, producing oscillatory microbubble flows with frequencies ranging from 1 to 200 Hz. Several geometrical variables can be tuned to enhance the performance of the fluidic oscillation process [6]. In a recent publication, the methods for micro and nanobubble generation were evaluated [10]. The geometrical parameters of the valve have been set to feed microalgae with a CO₂ concentrated exhaust gas in the form of dispersed microbubbles [11]–[12]. However, these valves have not been tested for other applications, due to the intricacies of the design. Indeed, depending on the application, the geometry of the device is modified to impose different bubbling regimes. Due to the complexity of the flow in these devices, a simulation stage is needed prior to fabrication. Thus, a reproducible modeling approach based on the detailed fluid transport phenomena is required. This is the main objective of the present study.

Fluid behavior inside micro diverter valve has been studied at the micro scale by means of CFD simulations due to the complexities involved: turbulence, compressibility, oscillation, unsteady state and size scale. Suitable and efficient CFD modeling makes possible to evaluate multiple conditions, reducing experimental work and development costs [13]. For example, the flow diverting process at low Reynolds numbers has been studied through CFD techniques [12]. Experimentally, the fluidic oscillator has been assessed in a

wind tunnel to understand the pressure recovery in the equipment, which directly affects the energy efficiency [14]. This feature reduced costs in the process, as compression costs are important in bioprocesses. CFD simulations have been compared against experimental results obtained from Particle Image Velocimetry (PIV) tests [15], demonstrating the possibility of using CFD modeling to increase the performance of the device. Mesh adaptation methods have been used to reduce the error associated with the mesh resolution and processing computation limit [15].

Despite the efforts made in recent years to evaluate valve performance by means of CFD simulations, detailed CFD numerical modeling and evaluation has not been performed due to the high computational requirements and complexity of turbulence behavior modeling in oscillating systems. An evaluation of mesh generation methods and a mesh independence analysis has not been carried out because this procedure involves a lengthy preprocessing time. Moreover, turbulence models, which may affect results and influence computation time, have not been assessed in detail. These reasons make this study an important one regarding the CFD modeling of the system, establishing a foundation for further development worldwide in several industrial applications.

This paper presents the CFD modeling evaluation of a bi-stable diverted valve at a Reynolds number of 3800 and a frequency of 200 Hz. First, two mesh generation methods were evaluated to simulate this valve at steady state condition. Then, a mesh independence analysis was carried out to find an adequate mesh size and a configuration with a reasonable computational time and accurate results. A brief analysis regarding time-step size using the Courant number approach was also performed. Subsequently, the transient behavior of the valve was reproduced and analyzed by simulating successive steady states, using the pseudo-steady state approach. Finally, results obtained using two turbulence models ($k-\epsilon$ Standard and RGN) were compared [16]–[17]. The behavior of the flow process in the system is presented. The results will be compared and validated using experimental data in a future publication.

2. EXPERIMENTAL DEVELOPMENT

MICRO-DIVERTER VALVE MODEL

The micro diverter valves presented have geometric characteristics that contribute to flow deflection [12]. First, the fluid enters the equipment through the supply terminal S (**Figure 1**). Second, the valve has a contraction that transforms pressure energy into kinetic energy; a lower pressure causes further flow deflection. Next, a recycled stream impinges upon the flow coming from the contraction, and causes its deflection.

Subsequently, in a pressure recovery expansion region, the flow attaches to one wall, and enough turbulence is generated to decrease the pressure in the opposite wall. This causes the main flow to exit the valve through the terminal close to the high-pressure region. At the same time, flow enters the valve through the terminal close to the low-pressure region, where the curved splitter nose diverts fluid layers back towards the outlet of the contraction. This holds the flow deflected before it moves to the opposite wall [15].

OPERATION AND BOUNDARY CONDITIONS

Industrial processes require the highest possible mass transfer, and this is achieved by reducing the bubble size. Microbubble diameter depends directly on the fluidic oscillation frequency. The valve operation frequency ranges from 1 to 200 Hz. The higher the frequency the lower bubble size [12]. Therefore, in this work a frequency of 200 Hz is used. At higher frequency, there are faster pressure changes in the equipment and it is more difficult to reproduce the fluid behavior in the valve. Experimental work shows pressure recovery occurs properly at Reynolds numbers higher than 10000 [14]. However the valve works properly at Reynolds numbers above 2000 [15]. In this work, a Reynolds number of 3800 was used.

This article evaluates the valve at best operating condition to divert 20 L per min of air (200 Hz). The velocity at the supply terminal S is 12 m/s (**Figure 1**). The pressure at outlets Y1 and Y2 is fixed at 0 Pa. In order to find stable states, the recycle was not considered

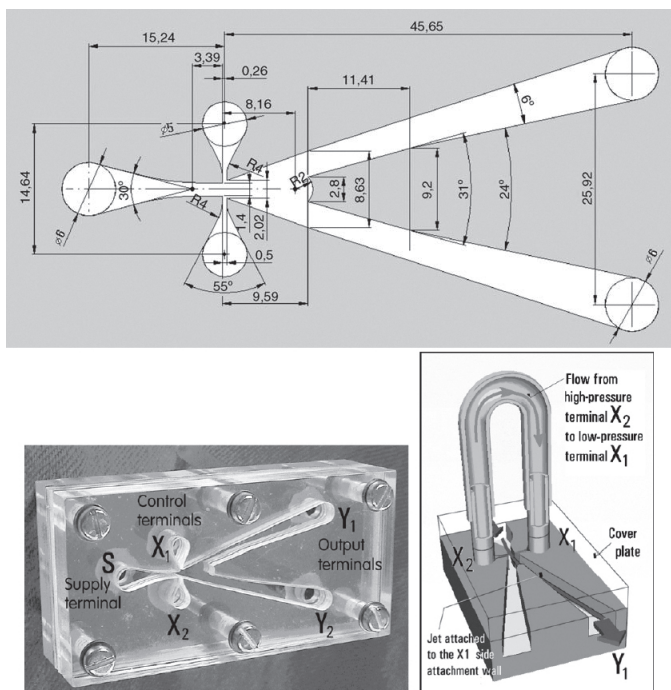


Figure 1. Valve geometry and dimensions[6], [10]–[12]

and control terminals X1 and X2 were replaced by walls. Later, the recycle was taken into account to simulate transient states.

MATHEMATICAL MODELS

Ansys-Fluent® was used to model the system (version 14.0). In Ansys-Fluent the finite volume method is used to solve continuity and momentum equations in tridimensional Cartesian coordinates over an unstructured tetrahedral mesh. The turbulent behavior was calculated using the two equation k-epsilon model in the standard and RNG formulations, and the latter model is suitable for handling “soft” swirling flows and low-Reynolds number effects [17]–[22]. Standard wall functions treatment was used to solve turbulence stresses, and the turbulence model constants were not modified.

Second order upwind for momentum, and first order upwind for turbulent kinetic energy and dissipation rate were implemented as discretization schemes. The SIMPLE algorithm was used for pressure-velocity coupling. The equations were solved using default under-relaxation factors, and they were adequate to solve continuity equations with residuals of 10^{-5} which are consistent with values reported elsewhere for similar simulations [15]. The simulations were carried out using high power hardware, and the main specifications of the workstation equipment used are as follows:

- 128 Gb RAM DDR3.
- Two processors: Intel® Xeon sixteen core 2.0 GHz.

MESH INDEPENDENCE ANALYSIS

In previous works, stationary states for the valve have been modeled to study the scalability properties of the equipment, in terms of dimensionless numbers, to analyze the pressure recovery inside the valve and to calculate the pressure difference that generates fluidic oscillation [12], [14]-[15]. Other studies have performed evaluations of accuracy for modeling in steady state fluid flows avoiding turbulent considerations, and this approach has made it possible to estimate the error associated with mesh performance [23]-[25]. In these works, steady states for the equipment were used to analyze pressure and velocity profiles using gradient adaptation refinement. If boundary conditions are not changed, this refinement method is suitable for calculating profiles in regions with abrupt changes. For problems with changing boundary conditions and flow oscillation, a gradient adaptation procedure would increase computational time due to the continuous change of gradient positions. Instead, the system can be modeled using a constant mesh over which different boundary conditions are imposed. This approach was used in this study.

Tetrahedral meshes were created using advanced size function. To increase control over cells sizes, the angle between normal vectors, the number of elements used in the gaps, and the progression between minimum and maximum cell size were changed[17]. The curvature, and proximity and curvature methods were employed. Patch conforming tetrahedrons were used for local control of the mesh.

These procedures were implemented to generate meshes with gradually increasing cell numbers ranging from 10×10^3 to 1500×10^3 elements. In order to evaluate mesh independence, errors were computed using equations (1) and (2).

$$v_{mass} = \frac{\sum_i^n v_i \rho_i V_i}{\sum_i^n \rho_i V_i} \quad (1)$$

$$\varepsilon_{\rho,rel} = \frac{v_{mass}(corser\ mesh) - v_{mass}(finest\ mesh)}{v_{mass}(finest\ mesh)} \quad (2)$$

Where v_{mass} is the mass weighted average velocity, and $\varepsilon_{p,rel}$ is the mass weighted velocity relative error of the domain, v_i is the velocity (L/T^3), ρ_i is the density (M/L^3), and V_i the volume of the cell i (L^3). A total of 18 meshes of different sizes were tested for the curvature method, and 14 for the proximity and curvature method. **Table 1** sets out a review of previous studies where different refinement methods were used to simulate this valve. As can be seen, meshes from 17×10^3 to 200×10^3 cells were evaluated. In this work, a wider number of cells were examined.

Table 1. Cells number and refinement methods used in different studies.

Author	Number of Cells	Refinement method
Tesař, V., C.-H. Hung, et al. (2006)	70×10^3	Not Reported
Tesař, V. (2009)	17×10^3 - 30×10^3	Gradient Adaptation
Tesař, V. and H. C. H. Bandalusena (2011)	150×10^3 - 200×10^3	Gradient Adaptation
This study	10×10^3 - 1500×10^3	Advanced size function and gradient adaptation methods

3. RESULTS AND ANALYSIS

MESH INDEPENDENCE ANALYSIS

Figure 2 shows that even at a low number of cells, the mass weighted velocity relative error is acceptable (less than 18%). Both cell size function methods, curvature and curvature and proximity, show that the error decreases when the number of cells increase. However, curvature and proximity shows a monotonic decreasing trend and thus this method was chosen for further evaluations.

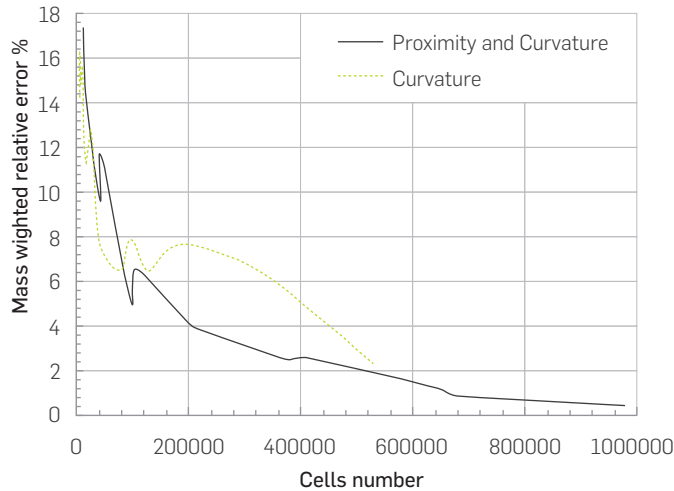


Figure 2. Mass wighted velocity relative error versus number of cells.

Figure 2 only shows the global error for the valve. Nonetheless in regions with abrupt gradients, errors may be higher and thus it is necessary to study these regions in greater detail. The results of these analyses are presented in Figure 3, which sets out the difference between velocity vectors obtained using a mesh of 681000 cells and coarser meshes in all regions of the valve. In order to compare velocity profiles obtained from different meshes, the velocity was interpolated [19]. The velocity differences at output terminal Y1 are small, and this is because the flow was low at that terminal. As expected, velocity differences are higher in regions with abrupt gradients as at the pressure recovery expansion region, and especially near the walls.

A velocity relative error, calculated using equation (3), was used to compare the results obtained from different meshes.

$$\varepsilon_{i,rel} = \frac{v_i (\text{corser mesh}) - v_i (\text{finest mesh})}{v_i (\text{finest mesh})} \quad (3)$$

Where $\varepsilon_{i,rel}$ is the velocity relative error at cell i . In specific regions, velocity relative errors decrease from 30 to 10% as the cells number increases. These errors are not significant and only occur in specific zones of the valve. Thus coarser meshes could be used to simulate this valve. Nevertheless, this study was accomplished using a regular commercial computer, and even if higher precision is required, this can be accomplished with the same computational power. A mesh with 681067 elements had a mass weighted velocity relative error lower than 1 % and was used in further simulations.

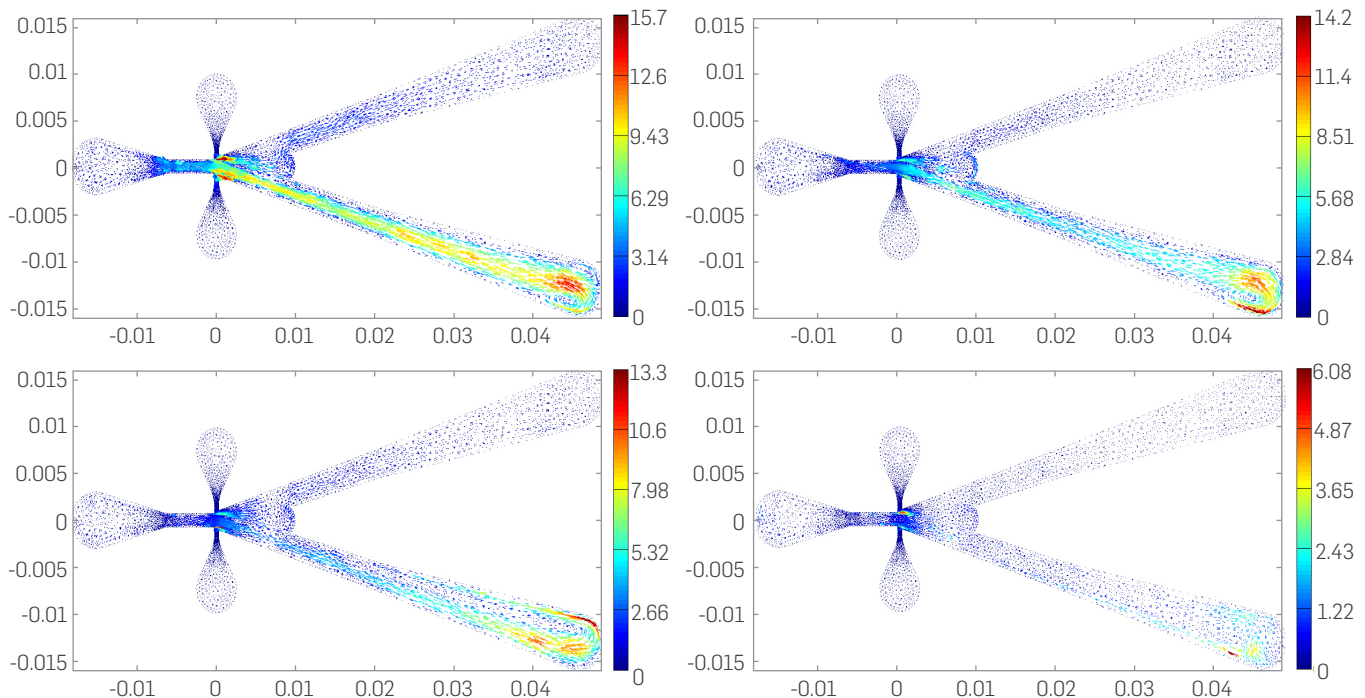


Figure 3. Velocity vectors difference (m/s) between the velocity profiles obtained using meshes of 12000 (Up-left), 41000 (Up-right), 106000 (Down-left), 368000 (Down-right), and a mesh of 681000 elements.

TIME-STEP ANALYSIS

A time-step analysis based on the Courant number approach was performed to establish the suitable time-step range for CFD simulations for this kind of flow device. The Courant number is defined as:

$$Co = \frac{v\Delta t}{\Delta x} \quad (4)$$

where v is the greatest velocity magnitude (50 m/s), in this case the maximum velocity expected inside the device at high Reynolds number values, Δt is the time-step in S, and Δx is the mean cell size (4.58×10^{-4} m). The recommended Co number values for the simulation to converge is: $5 < Co < 30$. This is according to the cases developed for similar flows reported in literature[17]–[19].

For this condition and the conditions mentioned above, it is possible to estimate the range of time-step for the simulations performed: $4.58 \times 10^{-5} \text{ s} < \Delta t < 2.75 \times 10^{-4} \text{ s}$. This range can be used as reference for the set-up of the simulations. Additional parameters, such as mesh size and computational power available must be considered. The analysis presented in this section could be used to reproduce the transient simulations of oscillatory turbulent high Re micro-scale flows, adding information that can be supplemented by other studies focused mainly on the numerical error due to mesh performance[23]–[25].

COMPARISON BETWEEN ADVANCE SIZE FUNCTION AND GRADIENT ADAPTATION MESH GENERATION METHODS

For problems with changing boundary conditions and flow oscillation, a gradient adaptation meshing method would increase computational time due to the continuous change of gradient positions. Since, in this study, states with different boundary conditions were simulated, advance size functions were used to simplify mesh generation. In this section, both mesh generation methods are compared. **Figure 4** shows interpolated vectors colored by velocity difference between the velocity profiles obtained using advance size function (681067 cells) and gradient adaptation methods (609000 cells). This figure shows that differences between both methods are small; the higher velocity relative errors are smaller than 8% and occur after the contraction nozzle. Therefore, usage of the advance function method is adequate to simulate the valve at different states and thus it was used in further simulations. It is important to mention that both methods have very similar average orthogonal qualities (0.84 and 0.86).

OSCILLATING FLOW DESCRIPTION

First, an attempt was made to simulate the flow at transient state using temporal discretization, the unsteady solutions methods, and the $\kappa - \varepsilon$ turbulence model. However, the flow oscillation was

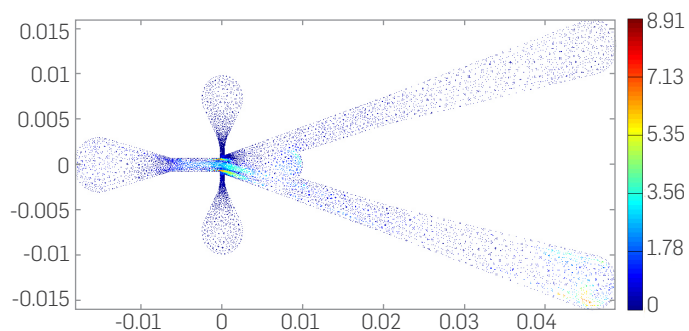


Figure 4. Velocity differences interpolated from advance size function and gradient adaptation mesh generation methods (m/s)

not observed even using the finest meshes. It seems that the $\kappa - \varepsilon$ turbulence model does not reproduce fine details of the turbulence generated in the valve. An advanced turbulence model could be used in future studies to describe the details of the turbulent phenomena.

In order to simulate the transient behavior of the equipment, a set of consecutive steady states were simulated[15]. The boundary conditions at terminal X1 and X2 were imposed using reported experimental data. To do this, the flow at one control terminal was increased for different steady states until the main flow diverted towards the opposite wall. Then, the recycle flow was decreased in that control terminal until zero. The same procedure was repeated in the opposite control terminal. A succession of these recycle flow pulses holds the flow oscillating continuously.

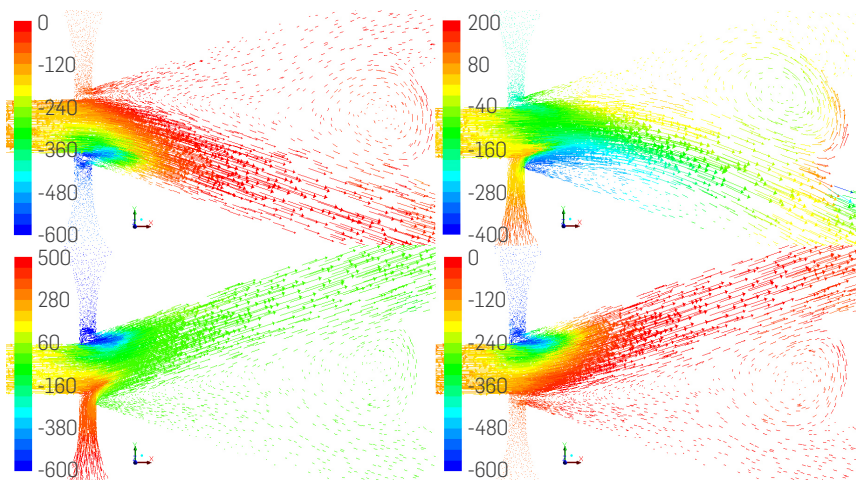


Figure 5. Pressure distribution at the pressure recovery expansion zone (Pa).

In a steady state simulation, depending on boundary and initial conditions, the main flow may attach to one wall or the other. **Figure 5** shows pressure distribution at the pressure recovery expansion zone for four states. As the velocity increases at the wall where the main flow is attached, the pressure decreases (**Figure 5**, upper-left). Then, the pressure gradient between the control terminals drives a flow toward the terminal where the main flow is attached (**Figure 5**, upper-right). This flow destabilizes and detaches the main flow. Later, the main flow diverts towards the opposite wall (**Figure 5**, lower-left). Subsequently, as the main flow attaches to the opposite

wall, the pressure profile inside the recycle inverts and the flow inside the recycle changes its direction from one control terminal to the other (**Figure 5**, lower-right).

Both valve outlets have nearly the same pressure. High turbulence at the pressure recovery expansion reduces pressure and causes oscillating flow entry at terminals Y1 or Y2. Main flow velocity at the inlet is 12 m/s and at terminals Y1 or Y2 it is near to 17 m/s. This increase is caused by pressure reduction in the equipment and the additional flow entering terminal Y1 or Y2.

The recycle acts as a feedback control loop that destabilizes, detaches and moves the main flow from one wall to the opposite wall. It acts as a signal transmitter that connects control terminals X1 and X2. Flow at the recycle is the control element, which is used to destabilize the main flow by imparting momentum on it. The velocity after contraction is higher and pressure is lower, thus a small change in pressure after the contraction can easily modify the main flow. The recycle control is enhanced by the geometry of the pressure recovery expansion as the detachment process is retarded by the action of streams deflected by the curved splitter nose [15].

Previous studies used Reynolds numbers from 800 – 15000. These studies proved that even at a low Reynolds number, the vortex in the pressure recovery expansion oscillates and the diverting process occurs. In this study, we used a Reynolds number of 3400, and the diverting process was observed as expected. At this Reynolds, a pressure loss of 1000 Pa was observed, and such pressure loss did not affect the diverting process. This pressure loss does not seem to be significant, however, if several valves are to be used in parallel or a series, consideration must be given to ensuring good hydraulic behavior in the system.

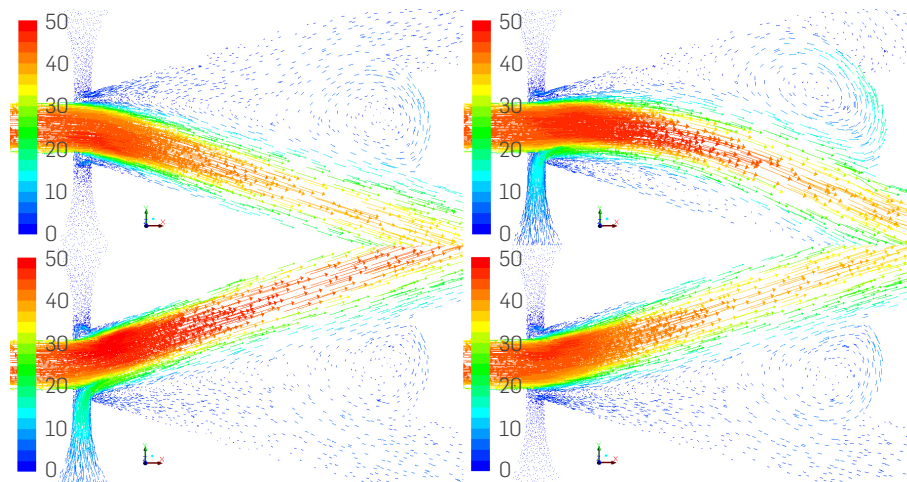


Figure 6. Velocity distribution at the pressure recovery expansion zone (m/s).

Figure 6 shows the velocity distribution at the pressure recovery expansion zone. The first state was simulated using walls as boundary conditions at the recycle terminals, thus fluid velocity in the terminals was zero (Up-left). Later, the velocity was increased gradually at the terminal next to the wall where the main flow was attached. The velocity of the recycled fluid was increased from 0 to 2.5 m/s, in steps of 0.12 m/s, until main flow was diverted to the other output terminal (down-left). After this happened, the velocity of the recycled fluid was decreased, using the same step, until zero (down-right). This process takes around 2.5 ms. At the end of the process, the velocity of the recycled fluid starts to increase at the

opposite terminal until an oscillation is completed. A supplementary video shows the process (Video 1 k epsilon RNG: <https://www.youtube.com/watch?v=GyW97mvbreo>).

COMPARISON OF $k - \epsilon$ STANDARD AND $k - \epsilon$ RNG TURBULENCE MODELS

The $\kappa - \epsilon$ standard model is a simple approach that can predict turbulent energy and its dissipation rate locally along the flow domain. However, this model is not suitable for rotating flows with large strains [8]. The $\kappa - \epsilon$ RNG formulation is effective to simulate small-scale turbulence inside expanding ducts with higher accuracies. Since $\kappa - \epsilon$ RNG is able to reproduce turbulence in more complex processes, it has been used to simulate intricate flow patterns inside expansion ducts. However, the computational cost of this model is higher than the $\kappa - \epsilon$ standard model. In this section, we aim to compare these two turbulence models.

Figure 7 shows the ratio of outlet flow to supply flow as a function of time. This figure shows that there is a 20% overflow at outlet terminals, and the opposite outlet provides this overflow. The entering flow moves to the low-pressure region of the pressure recovery expansion and helps to increase the momentum of the recycle flow. This is consistent with experimental overflows of 17% reported in other studies [15]. A comparison of $\kappa - \epsilon$ standard and $\kappa - \epsilon$ RNG results shows that both turbulence models predict the same mean behavior (**Figure 7**), however, $\kappa - \epsilon$ RNG reproduces the oscillating fluctuations over the mean. The main difference between both turbulence models is the computation time, as calculations with $\kappa - \epsilon$ standard required half the time required with the $\kappa - \epsilon$ RNG model. Therefore, the $k - \epsilon$ standard model is able to reproduce turbulence in the device at a lower computational cost.

Figure 8 shows the ratio of the recycled flow at terminals X1 and X2 to supply flow. Since information about the flow at terminals X1 and X2 was not available, this flow was linearly increased and decreased with time. The flow was increased until the main flow diverted. The simulations showed that the recycled flow must be 14 % of inlet flow to deflect the main flow; this result is higher than the 7 % reported in other studies [20]. This difference is due to the higher viscous effects occurring at the lower Reynolds number used in this article [17]–[19].

The results show a good qualitative representation of the oscillatory and highly unstable flow pattern. Velocity profiles of the transient simulations for both

turbulence models can be seen in:

Video 1 k epsilon RNG:

<https://www.youtube.com/watch?v=GyW97mvbreo>

Video 2 k epsilon standard:

https://www.youtube.com/watch?v=NhQ_jFvPwMY

This description of the system makes it possible to understand the microscale effect of the flow oscillations. This model can be used to tailor the properties of the micro diverter valve to sustain the fluid oscillation required in different bubbling regimes. A validation of this model will be presented in a future study.

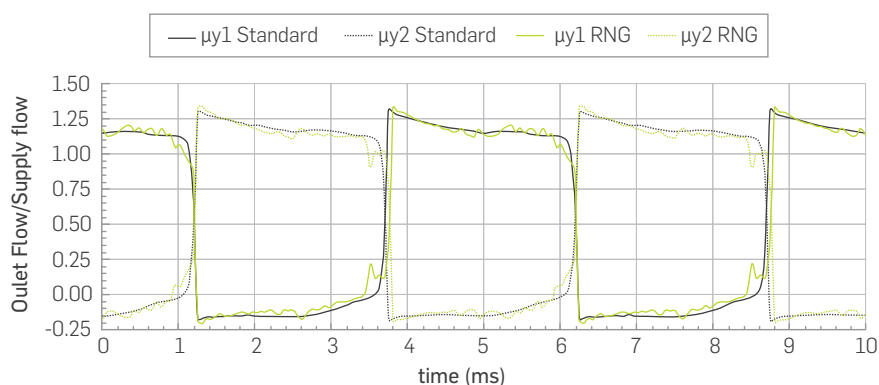


Figure 7. Ratio of outlet flow to supply flow as a function of time. Comparison of $\kappa - \epsilon$ standard and $\kappa - \epsilon$ RNG turbulence models ($\mu_y = \text{Outlet flow/Supply flow}$)

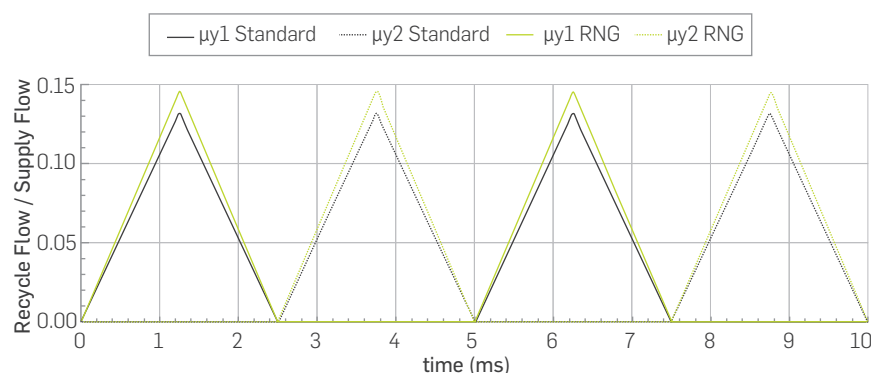


Figure 8. Ratio of recycled flow to supply flow as a function of time. Comparison of $\kappa - \epsilon$ standard and $\kappa - \epsilon$ RNG turbulence models ($\mu_x = \text{Recycle flow/Supply flow}$)

WALL FUNCTION y^+ ANALYSIS

The effect of the wall function y^+ , known as dimensionless wall distance, is discussed in this section. In the modern CFD modeling approaches of turbulent flow, the y^+ variable is not explicitly used. y^+ is a variable that can be calculated from CFD results. In other words, in the actual CFD modeling approach, y^+ , which makes it possible to model the boundary layer behavior in detail, is not used because it is a classic technique that limits the possibilities of mesh inflation and the capability of the CFD model to accurately reproduce pressure and velocity.

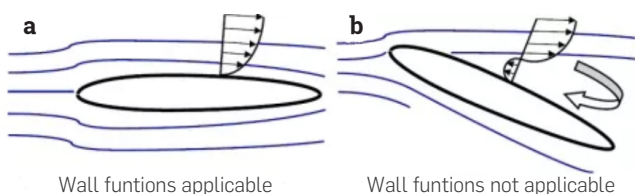


Figure 9. Applicability of wall functions: (a) Wall functions applicable case phenomena, and (b) Wall functions not applicable case phenomena. Taken from [26].

Furthermore, due to the non-stable nature of oscillating flow patterns in this study system it is not possible to use wall functions. This because the variability in the velocity fields cause the boundary layer size to change frequently in a way that cannot be described correctly by the wall function y^+ , and doing so would cause an error in the flow field, as can be seen in Figure 9b.

The implementation of any wall function will require further development in the boundary layer theory, making this classical approach suitable for this highly unstable oscillating flow modeling. Meanwhile the CFD modeling approach with high quality mesh performance is the best way to evaluate (in detail) the flow behavior to capture the boundary layer effects in detail.

CONCLUSIONS

The CFD modeling evaluation of a no-moving parts bi-stable diverted valve was presented. First, transient and steady state approaches were used to reproduce the fluid behavior in the valve. Different mesh configurations, mesh generation methods, and two turbulence models were evaluated to find the most adequate set-up to simulate this valve within reasonable computational times and acceptable errors. Finally, operation conditions at a low Reynolds (3800) and a high frequency (200 Hz) were used to assess other possible applications.

The evaluation of the mesh generation methods showed that both methods produce nearly the same results at steady state conditions. However, in transient state the gradient adaptation method would increase computational time due to the continuous mesh refinement caused by the change of gradient positions. Meshes from 10000 to 1600000 cells were used to evaluate the mesh independence. The errors observed between coarser and finer meshes are not significant and only occur in specific zones of the valve, thus coarser meshes could be used to simulate this valve. An estimated time-step range for the simulations performed was obtained: $4.58 \times 10^{-5} \text{ s} < \Delta t < 2.75 \times 10^{-4} \text{ s}$. This range can be used as reference to set-up the simulations. Additional parameters, such as mesh size and computational power available must be considered.

Transient flow in the micro diverter valve was simulated using temporal discretization, unsteady solution methods, and the $\kappa - \epsilon$ turbulence model. However, the flow oscillation was not observed in detail, even when using the finest meshes. The transient behavior of the equipment was evaluated using a set of consecutive steady states, with the recycled flow imposed as a boundary condition. The use of this approach showed that it is possible to reproduce the flow oscillation through consecutive steady states.

A comparison of $k-\epsilon$ standard and $\kappa - \epsilon$ RNG results shows that both turbulence models predict the same mean behavior. However, the $\kappa - \epsilon$ RNG reproduces the oscillating fluctuations around the mean. Nonetheless, calculations with $\kappa - \epsilon$ standard took half the time than the computation using the $\kappa - \epsilon$ RNG model. Therefore, the $k-\epsilon$ standard model is more adequate to simulate this valve with limited computational resources.

The results for this work also show that even at a low Reynolds number (3800) and a high frequency (200 Hz), the valve was able

to divert the fluid. Thus, this valve is a robust and flexible device that can be used in a wide number of industrial applications. CFD proved to be a powerful tool to evaluate different configurations reducing experimental work. The results show the qualitative behavior of the fluid phenomena involved in the system.

Further research is required to apply wall functions such as y^+ in a suitable manner for this case, without making conceptual mistakes in relation to inaccurate modeling, mainly in the boundary layer.

ACKNOWLEDGEMENTS

Acknowledgment is made to the company S&S-Smart and Simple Engineering-Colombia for providing the technical support to use Ansys-Fluent® for this project. Special thanks to ESSS-Colombia for their support and supplying the license used for the project's implementation.

REFERENCES

- [1] M. Mair, M. Bacic, and P. Ireland, "Switching Dynamics of a Fluid Diverter Valve Using Ultrasonic Excitation for Active Flow Control," 47th AIAA Fluid Dyn. Conf., no. June, pp. 1-14, 2017.
- [2] J. M. Peng, Q. Zhang, G. lin Li, J. W. Chen, X. Gan, and J. fu He, "Effect of geometric parameters of the bistable fluidic amplifier in the liquid-jet hammer on its threshold flow velocity," Comput. Fluids, vol. 82, pp. 38-49, 2013.
- [3] X. Zhang, J. Peng, D. Ge, K. Bo, K. Yin, and D. Wu, "Performance Study of a Fluidic Hammer Controlled by an Output-Fed Bistable Fluidic Oscillator," Appl. Sci., vol. 6, no. 10, p. 305, 2016.
- [4] R. Trybal, OPERACIONES DE TRANSFERENCIA DE MASA. McGraw-Hill, 1981.
- [5] R. Perry, J. Perry, and D. Green, Perry's Chemical Engineers' Handbook, 8th ed. McGraw-Hill, 2007.
- [6] W. B. Zimmerman, B. N. Hewakandamby, V. Tesař, H. C. H. Bandulasena, and O. A. Omotowa, "On the design and simulation of an airlift loop bioreactor with microbubble generation by fluidic oscillation," Food Bioprod. Process., vol. 87, no. 3, pp. 215-227, 2009.
- [7] V. Tesař, "Enhancing impinging jet heat or mass transfer by fluidically generated flow pulsation," Chem. Eng. Res. Des., vol. 87, no. 2, pp. 181-192, 2009.
- [8] N. D. Martin, M. Bottomley, and A. Packwood, "Switching of a Bistable Diverter Valve with Synthetic Jet Actuators," AIAA J., vol. 52, no. 7, pp. 1-5, 2014.
- [9] M. Mair, L.-W. Chen, J. Turner, M. Bacic, and P. Ireland, "Experimental and Numerical Study of a Piezo Driven Fluid Diverter for Active Flow Control," 52nd AIAA/SAE/ASME Jt. Propuls. Conf., pp. 1-16, 2016.
- [10] W. B. Zimmerman, V. Tesař, and H. C. H. Bandulasena, "Towards energy efficient nanobubble generation with fluidic oscillation," Curr. Opin. Colloid Interface Sci., vol. 16, no. 4, pp. 350-356, 2011.
- [11] W. B. Zimmerman, M. Zandi, H. C. Hemaka Bandulasena, V. Tesař, D. James Gilmour, and K. Ying, "Design of an airlift loop bioreactor and pilot scales studies with fluidic oscillator induced microbubbles for growth of a microalgae Dunaliella salina," Appl. Energy, vol. 88, no. 10, pp. 3357-3369, 2011.
- [12] V. Tesař, C. H. Hung, and W. B. Zimmerman, "Non-moving-part hybrid-synthetic jet actuator," Sensors Actuators, A Phys., vol. 125, no. 2, pp. 159-169, 2006.
- [13] G. Heng Yeoh and J. Tu, Computational Techniques for Multi-Phase Flows. ELSEVIER, 2010.
- [14] V. Tesař, "Mechanism of pressure recovery in jet-type actuators," Sensors Actuators, A Phys., vol. 152, no. 2, pp. 182-191, 2009.
- [15] V. Tesař and H. C. H. Bandulasena, "Bistable diverter valve in microfluidics," Exp. Fluids, vol. 50, no. 5, pp. 1225-1233, 2011.
- [16] NASA-Langley Research Center, "NASA-Turbulence Modeling Resource," 2017-03-08. [Online]. Available: turbomodels.larc.nasa.gov/.
- [17] M. Guevara and L. Belalcázar, "NGL supersonic separator: modeling, improvement, and validation and adjustment of $k-\epsilon$ RNG modified for swirl flow turbulence model," Rev. Fac. Ing., no. 82, pp. 82-93, 2017.
- [18] H. Versteeg and W. Malalasekera, An Introduction to Computational Fluid Dynamics The Finite Volume Method. Longman Scitific & Technical, 1995.
- [19] Ansys, ANSYS Engineering Analysis System User's Manual, 17th ed. Houston, 2016.
- [20] R. Bird, W. Stewart, and E. Lightfoot, Transport Phenomena, 2nd ed. 1958.
- [21] M. Guevara, J. Reyes, and F. Guevara, "Diseño y evaluación de un ciclón para separación de sólidos y gas de una corriente con un flujo multifásico empleando CFD," Rev. Virtual Pro, vol. 2, no. 166, 2015.
- [22] M. Guevara, "Diseño de un equipo de recuperación de líquidos de gas natural empleando CFD," Universidad Nacional de Colombia, 2015.
- [23] P. J. Roache, "Quantification of Uncertainty in Computational Fluid Dynamics," Annu. Rev. Fluid Mech., vol. 29, no. 1, pp. 123-160, 1997.
- [24] P. J. Celik, I. B., Ghia, U., and Roache, "Procedure for Estimation and Reporting of Uncertainty Due to Discretization in CFD Applications," J. Fluids Eng. ASME, vol. 130, no. 7, p. 78001, 2008.
- [25] P. J. Roache, "Perspective: a method for uniform reporting of grid refinement studies," Trans. Soc. Mech. Eng. J. Fluids Eng., vol. 116, 1994.
- [26] LEAP CFD Team, "Computational Fluid Dynamics (CFD) Blog - LEAP Australia & New Zealand | Tips & Tricks: Turbulence Part 2 - Wall Functions and Y^+ requirements," 2012. [Online]. Available: https://www.computationalfluidynamics.com.au/tips-tricks-turbulence-wall-functions-and-y-requirements/. [Accessed: 22-Sep-2017].

Geocientíficos del Instituto Colombiano del Petróleo - ICP han elaborado modelos geológicos, geofísicos y geoquímicos para soportar las decisiones exploratorias y de perforación en zonas complejas, de alta incertidumbre estructural.

Geoscientists from the Colombian Petroleum Institute - ICP have developed geological, geophysical and geochemical models to support exploratory and drilling decisions in complex areas of high structural uncertainty